Sulfur 1s near edge x-ray absorption fine structure spectroscopy of thiophenic and aromatic thioether compounds

3 AUTHORS, INCLUDING:

Shirin Behyan
University of British Columbia - Vancouver
8 PUBLICATIONS **42** CITATIONS

Stephen G Urquhart
University of Saskatchewan
84 PUBLICATIONS **1,737** CITATIONS

Sulfur 1s near edge x-ray absorption fine structure spectroscopy of thiophenic and aromatic thioether compounds

Shirin Behyan,[1] Yongfeng Hu,[2] and Stephen G. Urquhart[1,a)]

[1]*Department of Chemistry, University of Saskatchewan, Saskatoon, Saskatchewan S7N 5C9, Canada*
[2]*Canadian Light Source, University of Saskatchewan, Saskatoon, Saskatchewan S7N 0X4, Canada*

Thiophenic compounds are major constituents of fossil fuels and pose problems for fuel refinement. The quantification and speciation of these compounds is of great interest in different areas such as biology, fossil fuels studies, geology, and archaeology. Sulfur 1s Near-Edge X-ray Absorption Fine Structure (NEXAFS) spectroscopy has emerged as a qualitative and quantitative method for sulfur speciation. A firm understanding of the sulfur 1s NEXAFS spectra of organosulfur species is required for these analytical studies. To support this development, the sulfur 1s NEXAFS spectra of simple thiols and thioethers were previously examined, and are now extended to studies of thiophenic and aromatic thioether compounds, in the gas and condensed phases. High-resolution spectra have been further analyzed with the aid of Improved Virtual Orbital (IVO) and Δ(self-consistent field) *ab initio* calculations. Experimental sulfur 1s NEXAFS spectra show fine features predicted by calculation, and the combination of experiment and calculation has been used to improve the assignment of spectroscopic features important for the speciation and quantification of sulfur compounds. Systematic differences between gas and condensed phases are also explored; these differences suggest a significant role for conformational effects in the NEXAFS spectra of condensed species. © 2013 AIP Publishing LLC. [http://dx.doi.org/10.1063/1.4807604]

INTRODUCTION

Sulfur compounds are an environmentally significant constituent of fossil fuels.[1] The quality and utilization of fossil fuels depend on their sulfur content as sulfur combustion products can impede the performance of catalytic converters. The anthropogenic emission and combustion of sulfur compounds produces poisonous compounds such as H_2S, SO_2, and SO_3, with the consequent acidification of water.[2,3] Knowledge of the molecular composition of crude oil is needed to improve desulfurization and hydrogenation processes in the petroleum industries.[3]

Similarly, the application of coal beneficiation technologies is dependent on knowledge of the chemistry of sulfur in the coal. As thiophenic and thioether compounds are an important family of sulfur compounds in crude oil,[4–9] the study of this class of sulfur compounds is of keen analytical interest.
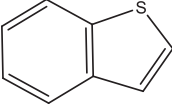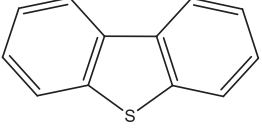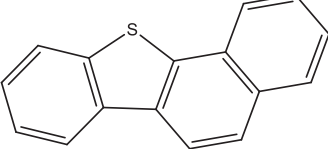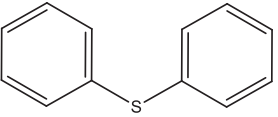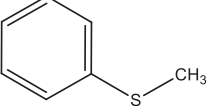
Near Edge X-ray Absorption Fine Structure (NEXAFS) spectroscopy is a powerful technique for studying the chemical form and quantity of sulfur species.[10] Sulfur 1s NEXAFS has been used for speciation and quantification of sulfur compounds in fossil fuels,[11–17] magmatic systems,[18] waterlogged wood from historical shipwrecks,[19] soils,[20] coal samples,[1] studies of the surface adsorption by thiol and thiolate species,[21–25] the sulfur chemistry of polymers,[26,27] photographic materials,[28] and in biological systems[29–32] such as study of biological transformation in cancerous cells.[33] The ratio of thiols to disulfides, which affects the functionality of many proteins, has been determined by sulfur 1s NEXAFS spectroscopy.[34] NEXAFS spectroscopy has been further extended to a microanalytical method with the development of X-ray microprobe and zone plate microscopy.[35–39]

In this work, the sulfur 1s NEXAFS spectra of the most relevant thiophenic and aromatic thioether species found in petroleum are studied in the gas, liquid, and condensed phases. These NEXAFS spectra have been further analyzed with the aid of *ab initio* Hartree-Fock calculations. The effect of phase on the NEXAFS spectra and the nature of Rydberg-valence mixing of transitions have also been studied.

In previous studies, spectral transitions of organosulfur compounds with different functionalities have been assigned on an empirical basis,[21,29,32,40–45] with some recent computational studies.[3,46–49] There have been few theoretical studies on sulfur 1s NEXAFS spectra of organosulfur compounds until recently.[3,46–54] Sulfur 1s NEXAFS calculations of organosulfur species have been reviewed in a recent study of aliphatic thioethers and thiols;[54] only studies relevant to this work are briefly mentioned here. Hitchcock *et al.*[49] used MS-Xα calculations to interpret spectral transitions in thiophene and thiolane species at sulfur 1s and 2p edges. Mijovilovich *et al.*[46] used density functional theory (DFT) calculations to show that ligand groups attached to a sulfur atom (phenyl versus benzyl, etc.) and with sulfur-sulfur bonding have a significant effect on the shape of the sulfur 1s NEXAFS spectra of sulfides and disulfides. Mijovilovich *et al.*[3] also simulated the sulfur 1s NEXAFS spectra of dibenzothiophene, dibenzothiophene sulfone, and DL-methionine at several different levels of DFT theory and compared these data to the experimental data. The authors concluded that

---
a)Author to whom correspondence should be addressed. Electronic mail: stephen.urquhart@usask.ca

Molecular structure	IUPAC name
	Thiophene
	1-Benzothiophene
	Dibenzo[b,d]thiophene
	Benzo[b]naphtho[2,1-d]thiophene
	1,1'-Sulfanediyldibenzene
	(Methylsulfanyl)benzene

SCHEME 1. Molecular drawings of thiophenic and unsaturated thioether compounds.

resolution of these compounds is difficult due to the similar energy of the main feature in the spectra of the different molecules.[3] Recently, the NEXAFS spectra of some organic and inorganic sulfur compounds have also been simulated theoretically by FEFF8 and WIEN97, showing that the combination of experiment and calculations can give useful information in mechanism of carcinogenesis.[53]

This work examines the sulfur 1s NEXAFS spectra of thiophenic and aromatic thioether compounds relevant to petroleum (see Scheme 1) in the gas, liquid, and solid phases and compares these data to a wider range of *ab initio* simulations. To select molecules, molecular symmetry, the identity of ligand groups attached to the sulfur atom, and the overall size of the molecules were considered. The results of *ab initio* Improved Virtual Orbital (IVO) and Δ(Self-Consistent Field (SCF)) calculations have been used to examine the degree of Rydberg-valence mixing, and to establish the assignments of features observed in the experimental spectra.

Gas phase spectra are free of solid-state broadening, and solid phase spectra can suffer from charging effects in the case of total electron yield detection or self-absorption in the case of fluorescent yield detection. However, the condensed phase spectra (liquid and solid phases) are more likely to represent a realistic picture of the spectroscopy of sulfur in analytical targets such as coal and petroleum. Gas phase compounds are examined for the simplicity of their assignments and their direct relationship to *ab initio* simulations. Condensed and liq-

uid phases are examined for the practical application of these spectra for sulfur speciation and quantification in fossil fuel studies, and as shown in this work, the important role of conformation effects.

COMPUTATIONAL METHODS

Ab initio calculations were performed by Kosugi's GSCF3 package.[55,56] This approach is based on the IVO approximation, which explicitly includes the core hole in the Hartree-Fock Hamiltonian. The IVO approximation has been proved to be effective at the simulation of core excitation spectra of organic and organometallic compounds at the carbon, nitrogen, oxygen, silicon, and sulfur 1s edges.[54–65] IVO calculations are particularly effective for transitions below and near the ionization potential (IP), where the sulfur 1s NEXAFS spectra show the strongest and most distinctive transitions.

The geometries used for these calculations (see Scheme 1) were provided by *ab initio* geometry optimization at the HF/6-31G* level, using the SPARTAN 06 program.[66] Frequency calculations were performed to ensure that the geometries were minimum structures (no imaginary frequencies) except for the additional conformational isomers of 1,1′-sulfanediyldibenzene, where a particular geometry was fixed and the remaining structural variables optimized. For the IVO calculations with GSCF3, the basis sets were similar to those used previously including:[54] hydrogen (41); second row atoms (carbon, nitrogen, and oxygen) (621 41); sulfur (with the core hole) (311111111 311111). Additional d polarization functions were placed on the sulfur atom ($\zeta_d = 0.183$ and $\zeta_d = 0.659$).

Simulated spectra were obtained from the IVO calculations by broadening each transition as a Gaussian line with the Simile2 package,[67] with the following energy dependent widths: 0.6 eV fwhm for bound states, 1.2 eV fwhm for states from the IP to 4 eV above the IP, and 4.0 eV fwhm for states more than 4.0 eV above the IP. These widths are chosen to track the experimental line width observed in the sulfur 1s NEXAFS spectra. The natural width of the sulfur 1s core shell is 0.59 eV,[68] although observed transitions are wider due to vibrational broadening and other excited state lifetime effects. Molecular orbital (MO) plots are provided for selected unoccupied orbitals.

The presence of Rydberg transitions, as well as Rydberg-valence mixing, should be considered in the interpretation of gas phase NEXAFS spectra. In the IVO approximation, the energies of Rydberg states are calculated more accurately than the valence state energies; therefore, spurious Rydberg-valence mixing can occur. This effect can be minimized in "Δ(SCF)" calculations where the screening effect of the excited electron is explicitly included. This process is performed for each excited state; for higher excited states, the shallower unoccupied orbitals are frozen to maintain orthogonality.[69–71] These Δ(SCF) calculations have been described in more detail elsewhere.[70,71] This approach was used by Kosugi *et al.*[72] to remove spurious Rydberg-valence mixing in the C 1s → σ^*(C–F) transitions of CH$_3$F, and was also used to

examine Rydberg-valence mixing in the NEXAFS spectra of gaseous[73] and condensed alkanes,[69] as well as amino acids.[58]

The degree of Rydberg character can be inferred by considering the orbital size and the energy difference between singlet and triplet core excited states for each transition (ΔE_{S-T}), as described previously.[69,73] For second row atoms, an ΔE_{S-T} energy difference of less than 0.05 eV and orbital size greater than 3 Å usually indicates some Rydberg character for the transition.[58,69,73] This trend was extrapolated for sulfur atom in determining the degree of Rydberg-valence mixing as well as the term values, and quantum defects of the Rydberg transitions.[74]

EXPERIMENTAL

All compounds (thiophene >99%, 1-benzothiophene (thianaphthene) 98%, dibenzo[b,d]thiophene (dibenzothiophene) 99%, benzo[b]naphtho[2,1-d]thiophene (1, 2-benzodiphenylene sulfide) 99%, (methylsulfanyl)benzene >99%, and 1,1′-sulfanediyldibenzene (diphenyl sulfide) 98%) were of reagent grade and purchased from Sigma Aldrich and used without further purification.

Experimental spectra of gas and condensed phases were obtained at the Canadian Light Source (CLS) on Soft X-ray Microcharacterization Beamline (SXRMB), using a Si(111) crystal monochromator which provides an energy resolution of 0.24 eV. Liquid and gas phase spectra were acquired when permitted by the physical properties of the species studied (vapor pressure, etc.). Gas samples (thiophene, (methylsulfanyl)benzene, and 1,1′-sulfanediyldibenzene) were introduced into a double gas cell (two gas cells in sequence) from the vapor pressure of the pure sample. The pressure inside the gas cell was in the range of 9.9-13.9 mTorr, below the pressure onset for saturation effects. A comparison of the spectra from the first and second gas cells was used to verify the absence of saturation. The experimental spectra of the gas phase molecules were recorded with total ion yield (TIY) detection mode.[75]

For solid samples (dibenzo[b,d]thiophene and benzo[b]naphtho[2,1-d]thiophene), a fine powder of the sample was spread homogeneously on a kapton tape (previously verified to be sulfur-free). For liquid and solid samples with a low melting point (1,1′-sulfanediyldibenzene, thiophene, 1-benzothiophene, and (methylsulfanyl)benzene), the sample was placed in a Teflon plate holder, which was then sandwiched by two layers of kapton tape. NEXAFS spectra were measured by fluorescence yield (FLY) detection with a Vortex 4-element Si(Li) drift detector, in a He filled chamber.

The TIY and FLY NEXAFS spectra were normalized by dividing each spectrum by an I_o spectrum, recorded simultaneously from an ion chamber upstream from the sample cell. The energy scale was calibrated to an absolute energy scale by setting the energy of the Ar $1s \rightarrow 4p$ transition to the value of 3203.54(10) eV, based on the absolute energy calibration of Breinig *et al.*[76] In previous work, the Ar $1s \rightarrow 4p$ transition energy was used to calibrate a weak contaminant signal (presumed to be $FeSO_4$) found on the Be windows of the ion chamber (calibrated value, 2481.62 eV). This signal, recorded

at the same time as all other spectra, was used as an internal calibration for these experiments.[54] The accuracy of this calibration is estimated to be ±0.3 eV, based on the ~0.7 eV lifetime broadening of the Ar $1s \rightarrow 4p$ transition used for the source calibration.

The calculated IVO sulfur $1s$ simulations always appear at lower energy than the experimental NEXAFS spectra because of strong relativistic effects for higher Z (third row) species.[2,52,54,77,78] In this paper, the experimental and theoretical data are presented on their own energy scales.

RESULTS AND DISCUSSION

Thiophenic compounds

Figures 1–4 present the experimental and simulated NEXAFS spectra of thiophenic compounds (thiophene, 1-benzothiophene, dibenzo[b,d]thiophene, and benzo[b]naphtho[2,1-d]thiophene), at two different levels of theory (IVO and Δ(SCF)). Figure 5 presents MO plots of the unoccupied molecular orbitals corresponding to the most intense pre-edge transitions in the Δ(SCF) spectra. Table I lists the energies and assignments for transitions observed in the experimental spectra. Table II presents the calculated energies, term values (term value = ionization potential − transition energy), ionization potentials, and the transition character for the features appearing below the ionization potential for both IVO and Δ(SCF) calculations. These results are reviewed on a molecule-by-molecule basis.
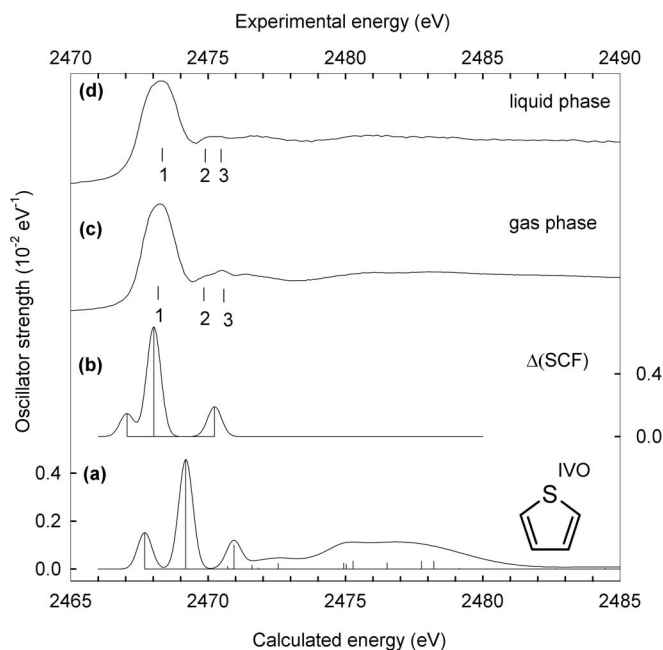

FIG. 1. Comparison of the experimental gas phase sulfur $1s$ NEXAFS spectrum of thiophene recorded by total ion yield, and the liquid phase spectrum recorded in fluorescence yield, to the simulated sulfur $1s$ spectra from *ab initio* IVO and Δ(SCF) calculations. (a) Simulated spectrum from IVO calculations; (b) simulated spectrum from Δ(SCF) calculations; (c) experimental spectrum recorded in the gas phase; (d) experimental spectrum recorded in the liquid phase.
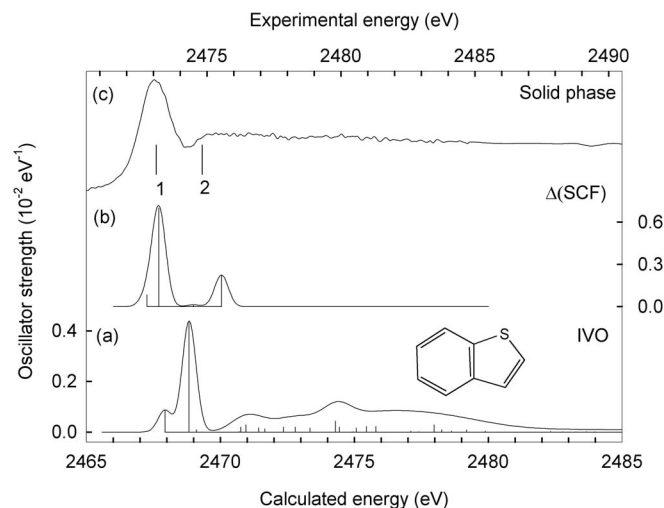
FIG. 2. Comparison of the experimental solid phase sulfur 1s NEXAFS spectrum of 1-benzothiophene, recorded in fluorescence yield, to the predicted sulfur 1s spectra from *ab initio* IVO and Δ(SCF) calculations. (a) Simulated spectrum from IVO calculations; (b) simulated spectrum from Δ(SCF) calculations; (c) experimental spectrum recorded in the solid phase.

Thiophene

Figure 1 presents the NEXAFS spectra of thiophene, acquired in gas and liquid phases, along with the simulated spectra from IVO and Δ(SCF) calculations. Energies and assignments of the most intense transitions are presented in Table I. The gas phase experimental spectrum consists of an intense white line at 2473.1 eV, followed by weak features at 2474.6 and 2475.2 eV. The white line of liquid phase spectrum is somewhat broader (2.0 eV fwhm compared to 1.5 eV fwhm for the gas phase spectrum), with broader features above the white line.

The simulated NEXAFS spectra differ from experiment in the character of the low energy transitions. The simulated spectra consist of weak, low energy feature, followed
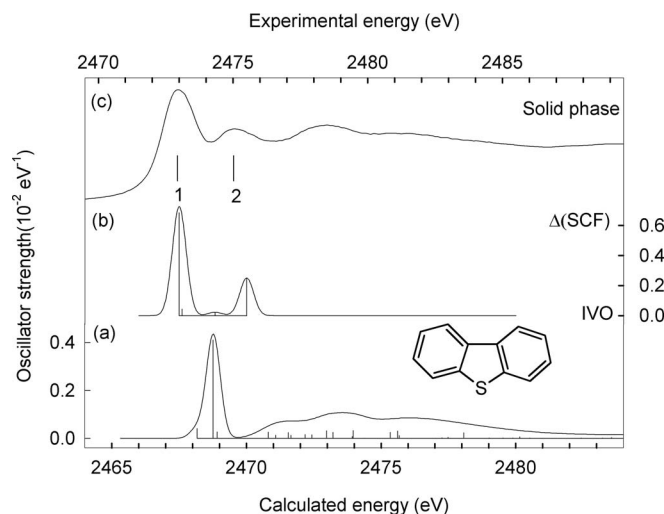

FIG. 3. Comparison of the experimental solid phase sulfur 1s NEXAFS spectrum of dibenzo[b,d]thiophene, recorded in fluorescence yield, to the predicted sulfur 1s spectra from *ab initio* IVO and Δ(SCF) calculations. (a) Simulated spectrum from IVO calculations; (b) simulated spectrum from Δ(SCF) calculations; (c) experimental spectrum recorded in the solid phase.

FIG. 4. Comparison of the experimental solid phase sulfur 1s NEXAFS spectrum of benzo[b]naphtho[2,1-d]thiophene, recorded in fluorescence yield, to the predicted sulfur 1s spectra from *ab initio* IVO and Δ(SCF) calculations. (a) Simulated spectrum from IVO calculations; (b) simulated spectrum from Δ(SCF) calculations; (c) experimental spectrum recorded in the solid phase.
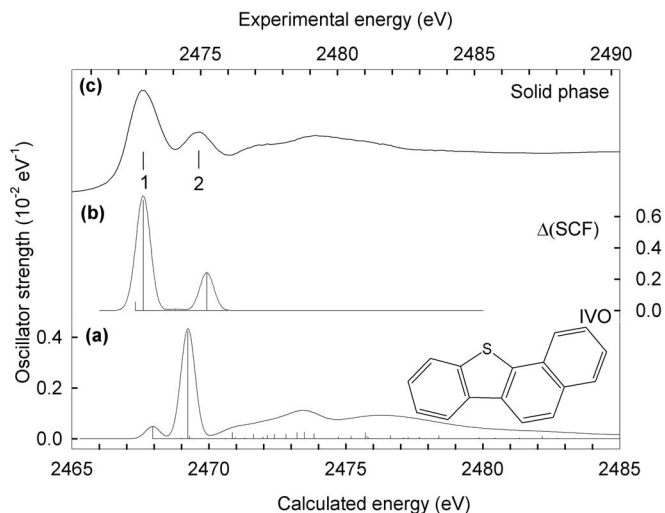
by a strong transition. However, the experimental spectra do not show a low energy shoulder. The low energy feature is 1.50 eV below the second transition in the IVO calculations; this energy difference should be resolvable in the experimental sulfur 1s NEXAFS spectra. This 1.50 eV energy difference between the first and second transitions in IVO calculations could arise from differences in the quality of calculated core-excited valence, Rydberg states, and mixed Rydberg-valence states. The intense low energy states were recalculated with the Δ(SCF) method, where screening effects in the core excited states are better accounted (see Computational Methods section). In the Δ(SCF) calculations, the energy difference between the first and the second excited states decreased to 0.98 eV. This smaller difference could be obscured by lifetime broadening in the experimental spectra, suggesting that both transitions overlap in the white line peak. The presence of the lower energy feature in the calculated spectra has been confirmed by the high quality calculations including Configuration Interaction (CI)[79] and Δ(SCF) calculations performed by Kosugi[70] as well as the angle dependent NEXAFS spectroscopy of thiophene.

MO diagrams of the major transitions observed in the simulated NEXAFS spectrum obtained in Δ(SCF) are presented in Figure 5(a). Based on the character of the LUMO orbital, the first transition in Δ(SCF) simulation is assigned as sulfur 1$s \rightarrow \pi^*$(S=C) character. The second transition in the simulation is to the σ^*(S–C) core excited state. The third transition, associated with the higher energy peak (3) in the experimental spectra, also has sulfur 1$s \rightarrow \sigma^*$(S–C) character that could be mixed with 4p Rydberg character based on the symmetry and the value of its quantum defect (see the supplementary material[74]). The white line observed in the experimental sulfur 1s NEXAFS spectrum of thiophene is assigned as an overlap of the lower energy sulfur 1$s \rightarrow \pi^*$(S=C) transition, and a slightly higher energy sulfur 1$s \rightarrow \sigma^*$(S–C)
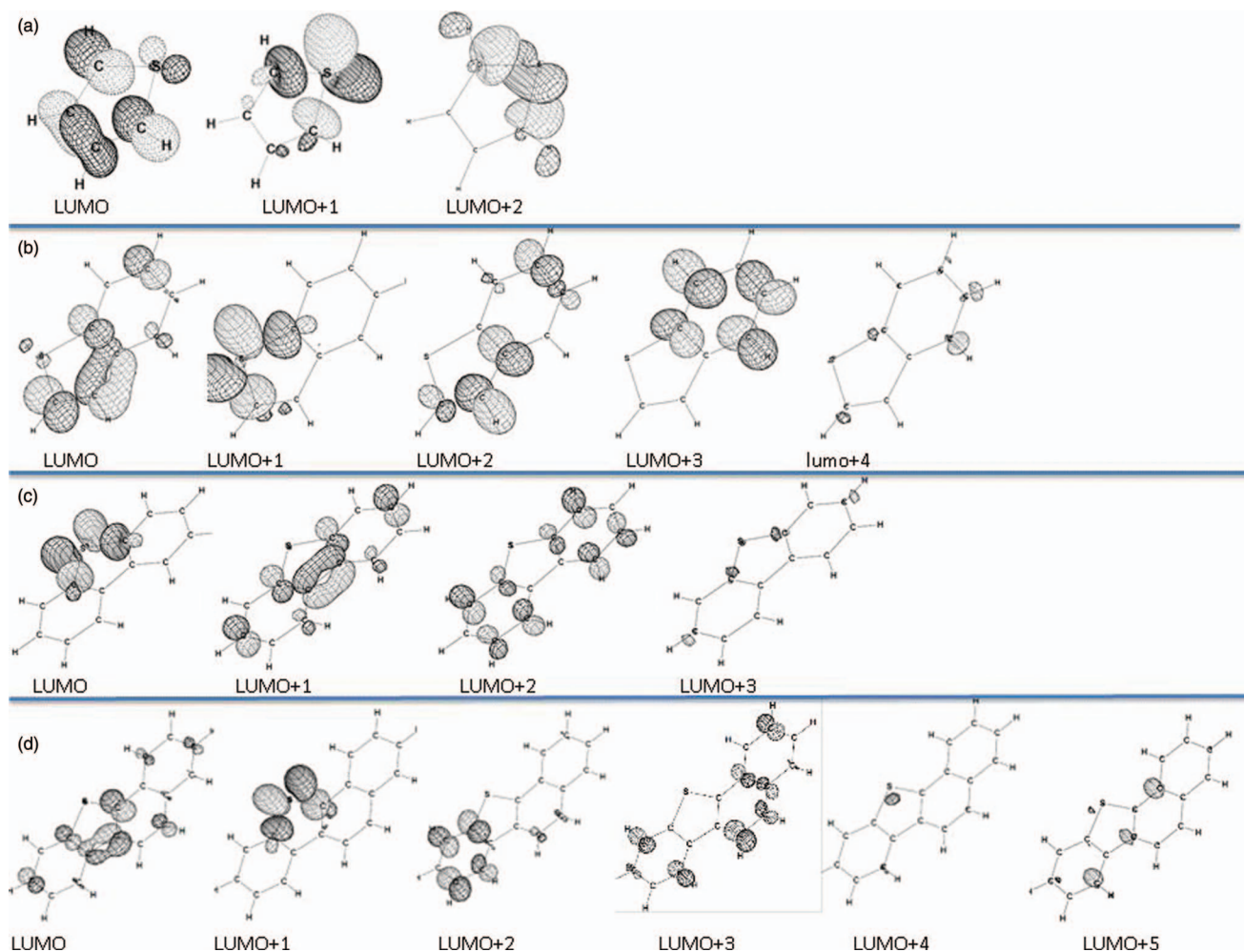
FIG. 5. Unoccupied molecular orbital diagrams obtained with Δ(SCF) calculations for the pre-edge features contributing to the simulated spectra (a) thiophene; (b) 1-benzothiophene; (c) dibenzo[b,d]thiophene; and (d) benzo[b]naphto[2,1-d]thiophene.

transition that is also confirmed by angle resolved NEXAFS spectroscopy and the CI calculations.[70,79] In previous assignments of the thiophene spectrum by Hitchcock *et al.*,[49] the second and the third peaks were assigned to sulfur $1s \rightarrow 4s$ and $4p$ Rydberg transitions, respectively. These calculations indicate that peak (3) also has σ^*(S–C) character in addition to $4p$ Rydberg character.

The liquid phase NEXAFS spectrum is broader than the gas phase spectrum, and edge position is shifted slightly to the higher energy relative to the gas phase spectrum. This energy shift is consistent with previous results obtained for the carbon $1s$ NEXAFS spectra of condensed neopentane relative to its gas phase spectra.[69] The broadening of the spectra in the condensed phase can arise from a decrease in core excited state lifetime because of quenching of the Rydberg character or an increased dissociative σ^*(S–C) character.[69]

1-Benzothiophene

A comparison of the experimental sulfur $1s$ NEXAFS spectrum of 1-benzothiophene in solid phase to simulated spectra from IVO and Δ(SCF) calculations is shown in

Figure 2. Energies and assignments of the most intense transitions are presented in Table I.

The solid phase experimental sulfur $1s$ spectrum of 1-benzeothiophene consists of an intense white line at 2472.9 eV, followed by a weak feature at 2474.5 eV, and very broad features in the continuum. Similar to thiophene, the simulated IVO NEXAFS spectrum differs from experiment in the presence of two lines at low energy: a weaker line, followed by a strong transition. The experimental spectrum does not show a low energy shoulder. In the IVO calculations, the low energy feature is 0.89 eV below the second transition, which should be resolvable in the experimental spectrum. This energy difference decreases to 0.44 eV in high quality Δ(SCF) calculations. This small difference could be obscured by lifetime broadening, suggesting that both transitions overlap in the white line peak in the experimental spectra.

The first transition in the Δ(SCF) simulation (Figure 5(b)) has π^*(S=C)/(C=C) character. The second transition is to a state with pure σ^*(S–C) character. Subsequent weak transitions, associated with the higher energy peak (2) in the experimental spectrum at 2474.5 eV, do not have clearly defined orbital character. The white line

TABLE I. Transition energies for the experimental sulfur 1s NEXAFS spectra of thiophene, 1-benzothiophene, dibenzo[b,d]thiophene, benzo[b]naphtho[2, 1-d]thiophene, (methylsulfanyl)benzene, and 1,1′-sulfanediyldibenzene.

Compound name	# Gas phase	Energy (eV) gas phase	# Liquid/solid phase	Energy (eV) liquid phase	Assignments
Thiophene	1	2473.1	1	2473.2	S $1s \rightarrow \pi^*$(S=C)
					S $1s \rightarrow \sigma^*$(S–C)
	2	2474.6	2	2474.9	4s
	3	2475.2	3	2475.3	S $1s \rightarrow \sigma^*$(S–C)/4p
1-Benzothiophene			1	2472.9	S $1s \rightarrow \pi^*$(S=C)/(C=C)
					S $1s \rightarrow \sigma^*$(S–C)
			2	2474.5	S $1s \rightarrow \pi^*$(C=C)
Dibenzo[b,d]thiophene			1	2472.8	S $1s \rightarrow \pi^*$(S=C)/(C=C)
			2	2474.9	S $1s \rightarrow \sigma^*$(S–C)
Benzo[b]naphtho[2,1-d]thiophene			1	2472.8	S $1s \rightarrow \pi^*$(S=C)/(C=C) and
					S $1s \rightarrow \sigma^*$(S–C)
			2	2474.8	Poorly defined
(Methylsulfanyl)benzene	1	2472.5			S $1s \rightarrow \sigma^*$(S–C)/π^*(C=C)
	2	2473.4			S $1s \rightarrow \sigma^*$(S–C)/π^*(C=C)
	3	2474.5			S $1s \rightarrow \sigma^*$(S–C)
1,1′-Sulfanediyldibenzene	1	2472.1	1	2472.5	S $1s \rightarrow \sigma^*$(S–C)/π^*(C=C)
	2	2473.1	2	2473.9	S $1s \rightarrow \pi^*$(C=C)
	3	2474.1			S $1s \rightarrow \pi^*$(C=C)

in the sulfur 1s NEXAFS spectrum of 1-benzothiophene is assigned as an overlap of the lower energy sulfur $1s \rightarrow \pi^*$ character from the 1-benzothiophene ring, and a slightly higher energy sulfur $1s \rightarrow \sigma^*$(S–C) transition. The second peak is assigned to sulfur $1s \rightarrow \pi^*$(C=C) transition.

Dibenzo[b,d]thiophene

Figure 3 presents the solid phase NEXAFS spectrum of dibenzo[b,d]thiophene, compared to the simulated spectra from IVO and Δ(SCF) calculations. Energies and assignments for spectral transitions are presented in Table I.

The solid phase experimental spectrum consists of an intense white line at 2472.8 eV, and a weak peak at 2474.9 eV followed by broad features in continuum. The experimental spectrum is the most similar to the Δ(SCF) simulated spectrum.

MO diagrams of the major transitions for simulated Δ(SCF) spectrum are presented in Figure 5(c). Based on the character of the LUMO orbital, the first transition in the Δ(SCF) simulation has sulfur $1s \rightarrow \sigma^*$(S–C) character, while the weak second transition has sulfur $1s \rightarrow \pi^*$(S=C)/π^*(C=C) character. The third transition in the simulation has sulfur $1s \rightarrow \pi^*$(C=C) character. The fourth transition is to σ^*(S–C) core excited state, which corresponds to peak (2) in the experimental spectrum.

The white line in the sulfur 1s NEXAFS spectrum of dibenzo[b,d]thiophene can be assigned as an overlap of the low energy sulfur $1s \rightarrow \sigma^*$(S–C) core excited state and a slightly higher energy sulfur $1s \rightarrow \pi^*$ molecular orbital of the two aromatic rings and the second peak is assigned to σ^*(S–C) state. In this molecule, the Δ(SCF) calculations reproduce the experiment better than the IVO calculations, in terms of the shape and energy splitting of the transitions.

Benzo[b]naphtho[2,1-d]thiophene

Figure 4 presents the comparison of experimental NEXAFS spectrum of benzo[b]naphtho[2,1-d]thiophene in solid phase to the simulated NEXAFS spectra from IVO and Δ(SCF) calculations. The major transitions and assignments of the experimental spectrum are presented in Table I.

The experimental solid phase spectrum of benzo[b]naphtho[2,1-d]thiophene consists of an intense white line transition at 2472.8 eV, followed by a low intensity high-energy transition at 2474.8 eV and broad features in the continuum. This spectrum is similar to the experimental spectrum of dibenzo[b,d]thiophene. Figure 4(b) shows that the simulated NEXAFS spectrum obtained in Δ(SCF) calculations is the most similar to the experimental spectrum.

In IVO calculations, the energy difference between the first and second transitions is about 1.04 eV, which should be resolved by experiment. In high quality Δ(SCF) calculations, this energy difference has been decreased to 0.30 eV, so it is reasonable that the low energy feature is not resolved.

Based on the shape of the unoccupied molecular orbitals corresponding to the dominant transitions from Δ(SCF) calculations (Figure 5(d)), the first transition in the simulation has sulfur $1s \rightarrow \pi^*$(S=C)/π^*(C=C) character. The second transition has pure σ^*(S–C) character, and subsequent transitions have π^*(C=C) character except the last two transitions which are difficult to classify within a simple π^* or σ^* picture.

The white line of the experimental spectrum is assigned as an overlap of the sulfur $1s \rightarrow \pi^*$ transition (where the π^* MO is delocalized over the aromatic rings) with the higher energy σ^*(S–C) excited states. Peak (2) is poorly understood on a simple π^* or σ^* basis.

In the study of the sulfur 1s NEXAFS spectra of a group of thiophenic compounds relevant to petroleum, it

TABLE II. Calculated energies, term values, ionization potentials, and assignments for sulfur $1s$ transitions appearing below the ionization potential for (a) thiophene, (b) 1-benzothiophene, (c) dibenzo[b,d]thiophene, (d) benzo[b]naphtho[2,1-d]thiophene, (e) (methylsulfanyl)benzene, and (f) 1,1′-sulfanediyldibenzene from *ab initio* IVO and Δ(SCF) calculations.

#	Ionization potential	Energy (eV)	Term value (eV)	Oscillator strength	Assignment	Energy (eV)	Term value (eV)	Oscillator strength
		(a) Thiophene Δ(SCF)				Thiophene (IVO) IP = 2470.974 eV		
LUMO	2471.642	2467.045	4.597	0.0009396	S $1s\rightarrow\pi^*$(S=C)	2467.663	3.311	0.0009739
LUMO+1	2472.210	2468.021	4.189	0.0044561	S $1s\rightarrow\sigma^*$(S–C)	2468.971	2.003	0.0029614
LUMO+2	2471.971	2470.238	1.733	0.0012207	S $1s\rightarrow\sigma^*$(S–C)/$4p$	2470.644	0.330	0.0000804
		(b) 1-benzothiophene Δ(SCF)				1-benzothiophene IVO, IP = 2470.575 eV		
LUMO	2471.532	2467.261	4.271	0.0005360	S $1s\rightarrow\pi^*$(S=C)/π^*(C=C)	2467.933	2.642	0.0005540
LUMO+1	2472.132	2467.702	4.430	0.0044707	S $1s\rightarrow\sigma^*$(S–C)	2468.827	1.748	0.0027757
LUMO+2	2471.593	2468.992	2.601	0.0000422	S $1s\rightarrow\pi^*$(C=C)	2469.114	1.461	0.0000606
LUMO+3	2471.593	2468.992	2.601	0.0000422	S $1s\rightarrow\pi^*$(C=C)	2470.700	−0.125	0.0000272
LUMO+4	2472.004	2470.042	1.962	0.0014345	Poorly defined	2470.759	−0.184	0.0002590
		(c) Dibenzo[b,d]thiophene Δ(SCF)				Dibenzo[b,d]thiophene IVO, IP = 2470.322 eV		
LUMO	2471.996	2467.496	4.5	0.0043827	S $1s\rightarrow\sigma^*$(S–C)	2468.168	2.154	0.0002677
LUMO+1	2470.989	2467.606	3.383	0.0002820	S $1s\rightarrow\pi^*$(S=C)/π^*(C=C)	2468.764	1.558	0.0026241
LUMO+2	2470.840	2468.833	2.045	0.0001428	S $1s\rightarrow\pi^*$(C=C)	2468.915	1.407	0.0001726
LUMO+3	2471.877	2470.008	1.869	0.0015955	Poorly defined	2469.336	0.986	0.0000000
		(d) Benzo[b]naphtho[2,1-d]thiophene Δ(SCF)				Benzo[b]naphtho[2,1-d]thiophene IVO, IP = 2470.275		
LUMO	2471.069	2467.319	3.750	0.0003540	S $1s\rightarrow\pi^*$(S=C)/π^*(C=C)	2467.933	2.342	0.0003127
LUMO+1	2472.087	2467.614	4.473	0.0045006	S $1s\rightarrow\sigma^*$(S–C)	2468.976	1.299	0.0000220
LUMO+2	2471.353	2468.787	2.566	0.0000511	S $1s\rightarrow\pi^*$(C=C)	2469.038	1.237	0.0027307
LUMO+3	2471.268	2468.962	2.306	0.0000002	S $1s\rightarrow\pi^*$(C=C)	2469.279	0.996	0.0000640
LUMO+4	2471.988	2469.922	2.066	0.0015463	Poorly defined	2470.591	−0.316	0.0000256
LUMO+5	2471.077	2470.695	0.382	0.0000027	Poorly defined	2470.779	−0.504	0.0003162
		(e) (Methylsulfanyl)benzene Δ(SCF)				(Methylsulfanyl)benzene IVO, IP = 2469.843 eV		
LUMO	2471.047	2467.169	3.878	0.0026386	S $1s\rightarrow\sigma^*$(S–C)/π^*(C=C)	2467.766	2.077	0.0009825
LUMO+1	2471.741	2468.035	3.706	0.0018383	S $1s\rightarrow\sigma^*$(S–C)	2468.833	1.010	0.0000028
LUMO+2	2470.896	2468.674	2.222	0.0000023	S $1s\rightarrow\pi^*$(C=C)	2468.993	0.850	0.0015440
LUMO+3	2470.789	2468.75	2.039	0.0009145	S $1s\rightarrow\sigma^*$(S–C)	2469.365	0.478	0.0012687
LUMO+4	2470.430	2469.845	0.585	0.0000551	S $1s\rightarrow\sigma^*$(S–C)	2469.643	0.200	0.0002515
		(f) 1,1′-sulfanediyldibenzene Δ(SCF)				1,1′-sulfanediyldibenzene IVO, IP = 2469.856		
LUMO	2471.303	2467.35	3.953	0.0034235	S $1s\rightarrow\sigma^*$(S–C)/π^*(C=C)	2468.181	1.675	0.0012648
LUMO+1	2471.049	2467.906	3.143	0.0003734	S $1s\rightarrow\pi^*$(C=C)	2468.245	1.611	0.0000040
LUMO+2	2470.570	2468.716	1.854	0.0004787	S $1s\rightarrow\sigma^*$(S–C)	2468.833	1.023	0.0001509
LUMO+3	2470.484	2469.267	1.217	0.0000137	S $1s\rightarrow\pi^*$(C=C)	2469.298	0.558	0.0000237
LUMO+4	2470.588	2469.474	1.114	0.0006801	S $1s\rightarrow\pi^*$(C=C)	2469.900	−0.044	0.0014770
LUMO+5	2470.687	2469.753	0.934	0.0009975	Poorly defined	2470.167	−0.311	0.0006728

has been observed that the liquid phase spectrum of thiophene is slightly different from the gas phase spectrum and is shifted to higher energy. The white lines of all of the experimental spectra are assigned as an overlap of sulfur $1s \rightarrow \sigma^*$(S–C) and π^* transitions. The Rydberg character is more pronounced in small molecules such as thiophene, and this Rydberg character likely decreases as the molecule size increases. The relative intensity of the π^* transition decreases as the molecule size increases, and this transition shifts to higher energy relative to the dominant sulfur $1s \rightarrow \sigma^*$(S–C) transition.

The second distinctive peak (2) observed in all the thiophene experimental spectra becomes more distinct in the larger thiophene heterocycles. This transition does not have a clearly defined orbital character. The higher energy above the white line could indicate some 2-electron transition character.

Aromatic thioethers

The sulfur $1s$ NEXAFS spectra of simple aliphatic thioethers has been previously reported.[54] This work extends these studies to unsaturated thioethers: (methylsulfanyl)benzene and 1,1′-sulfanediyldibenzene, because of their relationship to the aromatic thiophenes. The experimental spectra are compared to IVO simulations.

(Methylsulfanyl)benzene

Figure 6(a) represents the gas phase spectrum of (methylsulfanyl)benzene, along with the simulated spectra from IVO
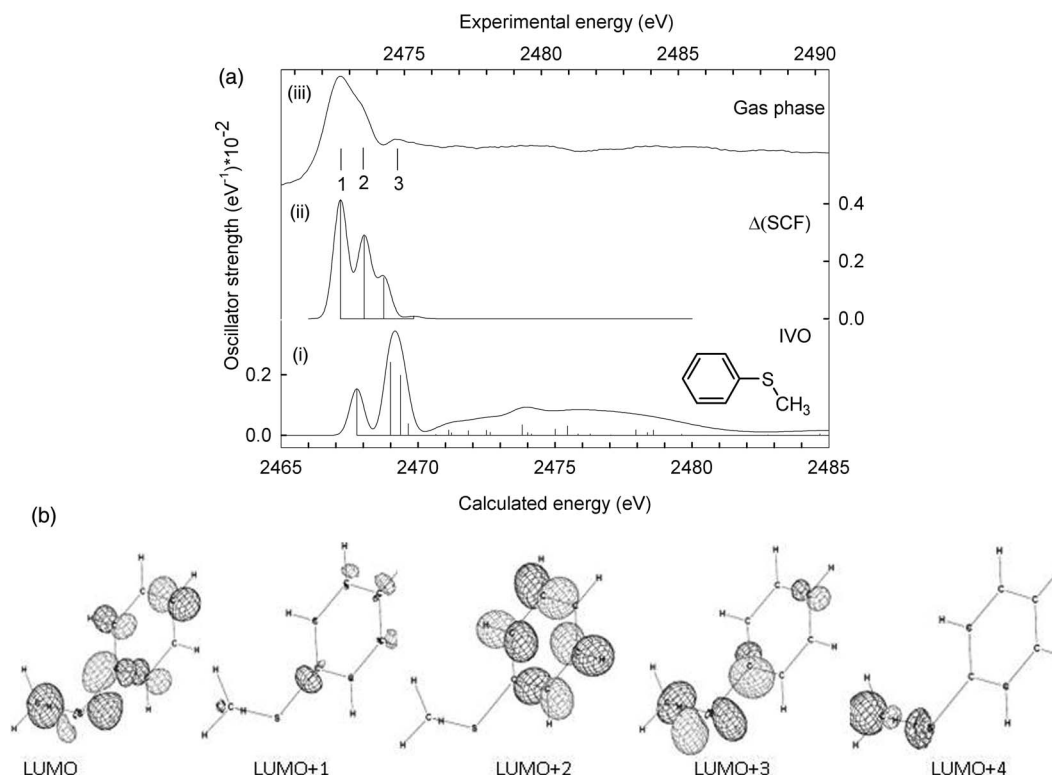
FIG. 6. (a) Comparison of the experimental gas phase sulfur 1s NEXAFS spectrum of (methylsulfanyl)benzene, recorded by total ion yield, to the predicted sulfur 1s spectra from *ab initio* IVO and Δ(SCF) calculations. (i) Simulated spectrum from IVO calculations; (ii) simulated spectrum from Δ(SCF) calculations; (iii) experimental spectrum recorded in the gas phase. (b) Unoccupied molecular orbital diagrams for the strong features contributing to the simulated spectra obtained from Δ(SCF) calculations.

and Δ(SCF) calculations. Energies and assignments of the most intense transitions are presented in Table I.

The experimental gas phase spectrum consists of an intense white line at 2472.5 eV, a higher energy shoulder at 2473.4 eV, followed by a weak high-energy peak at 2474.5 eV (peak 3), and broad features in the continuum. The white line of the experimental spectrum differs from the IVO simulation as two bands are observed in IVO simulation and three closely spaced transitions in the Δ(SCF) simulation. The low energy transition in the IVO simulation is stronger than in the thiophene simulations. The gas phase experimental spectrum is the most similar to the Δ(SCF) spectrum.

Based on the character of the unoccupied MOs (Figure 6(b)), the first transition in the experimental spectrum is assigned as sulfur $1s \rightarrow \sigma^*(S–C)/\pi^*(C=C)$ excited state. The higher energy shoulder (peak 2) consists of the overlap of sulfur 1s to $\sigma^*(S–C)$ and $\pi^*(C=C)$ character, and the third transition has a pure $\sigma^*(S–C)$ character. The shape of NEXAFS spectrum is similar to the previously studied aliphatic thioethers.[54] The spectral transitions in this molecule have an additional π^* character as a result of phenyl substituent, compared to methyl group in dimethyl sulfide.[54]

1,1′-Sulfanediyldibenzene

Figure 7 represents the gas and liquid phase spectra of 1,1′-sulfanediyldibenzene and compares these spectra to IVO simulations obtained for different conformational isomers.

The experimental gas phase spectrum of 1,1′-sulfanediyldibenzene consists of an intense white line at 2472.1 eV, and a higher energy shoulder at 2473.1 eV, followed by a weak feature at 2474.1 eV and broad features in continuum. The liquid phase spectrum consists of an intense peak at 2472.5 eV, followed by a second peak at 2474.1 eV, and broad features in continuum. The liquid phase spectrum is different from the gas phase spectrum in having two intense peaks instead of one peak with higher energy shoulders in the gas phase spectrum.

The gas phase spectrum is the most similar to the Δ(SCF) simulation for the equilibrium geometry (conformer 1 in Figure 2). The difference between the gas and liquid phase spectrum could suggest the presence of a range of conformers in the liquid phase. Several different conformers were investigated, in addition to the equilibrium geometry. One potential conformer (conformer 2 in Figure 7) has the two phenyl rings with the same tilt while another conformer (conformer 3 in Figure 7) has the two phenyl rings in the same plane. The Δ(SCF) simulation of conformer 2 is the most similar to the liquid phase spectrum, but the liquid phase spectrum is probably a combination of conformers.

Comparison of the Δ(SCF) simulations for the two conformers (see Figures 7(c) and 7(d)) to the liquid phase spectrum shows distinct changes. The intensity of a band at ∼2469 eV on the calculated energy scale (corresponding to the peak (2) in the liquid phase spectrum) increases and
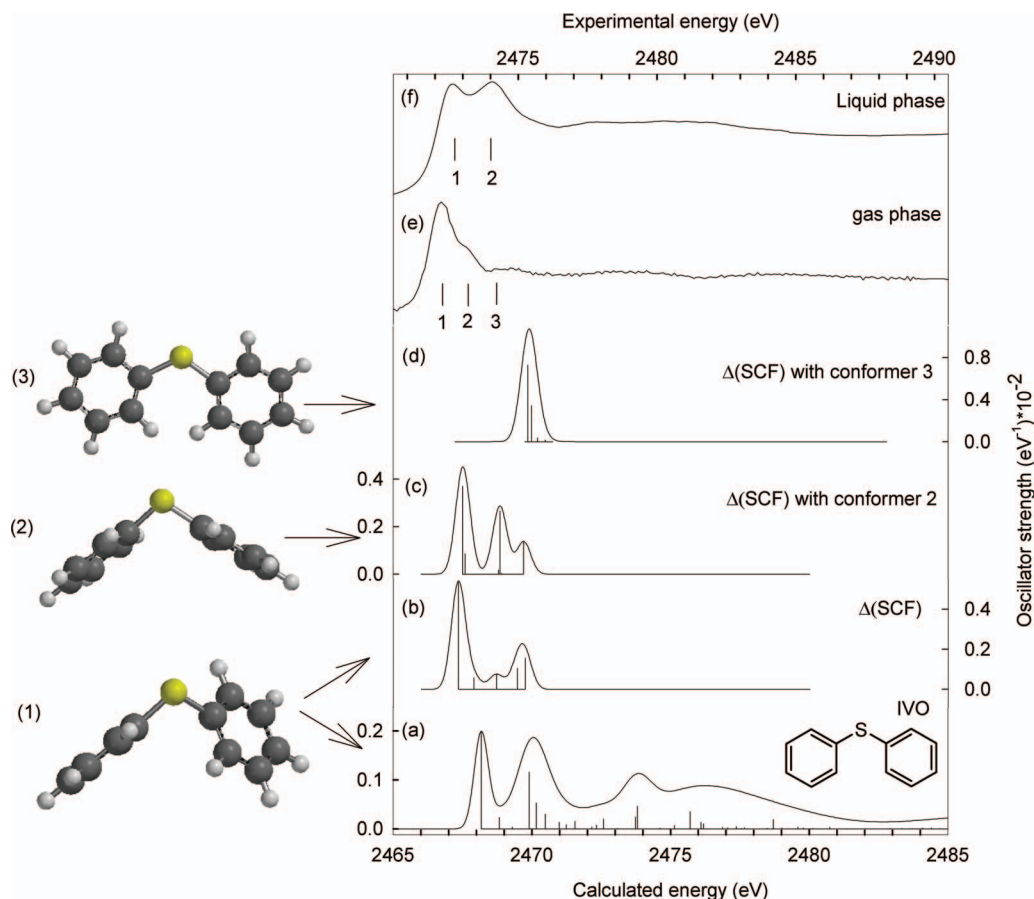
FIG. 7. Comparison of experimental gas phase sulfur 1s NEXAFS spectrum of 1,1′-sulfanediyldibenzene, recorded by total ion yield, and in liquid phase, recorded in fluorescence yield, to the predicted sulfur 1s spectra from *ab initio* IVO and Δ(SCF) calculations. (a) Simulated spectrum from IVO calculation with the equilibrium geometry (conformer 1); (b) simulated spectrum from Δ(SCF) calculations of the equilibrium geometry (conformer 1); (c) simulated spectrum from Δ(SCF) calculations of conformer 2; (d) simulated spectrum from Δ(SCF) calculations from conformer 3; (e) experimental spectrum recorded in the gas phase; (f) experimental spectrum recorded in the liquid phase.

reaches a maximum in flat geometry while the intensity of the first peak decreases. The different shape of peak 2 in the liquid phase spectra could be due to the presence of different conformers in the liquid phase while the gas phase spectrum should be most similar to the equilibrium geometry.

The MO diagrams of the major transitions for Δ(SCF) spectrum at equilibrium geometry are presented in Figure 8(a). Based on the shape of the unoccupied molecular orbitals, the first transition of the spectrum (Figure 7(b)) has sulfur $1s \rightarrow \sigma^*(S–C)/\pi^*(C=C)$ character. The third transition is to $\sigma^*(S–C)$ excited state and the subsequent transitions have sulfur $1s \rightarrow \pi^*(C=C)$ character. The third transition is not understood on a simple σ^* or π^* basis.

The first peak of the experimental spectra is assigned as an overlap of sulfur $1s \rightarrow \sigma^*(S–C)$, and $\pi^*(C=C)$ character, and the second transition in the liquid phase and peak (4) in the gas phase as sulfur $1s \rightarrow \pi^*(C=C)$ excited state. The shape of the gas phase spectrum is similar to the aliphatic thioethers, but with a difference in the shape of liquid phase spectrum.

The sulfur 1s NEXAFS spectra of aromatic thioethers were examined by experimental and IVO simulations. The shape of the NEXAFS spectra of aromatic thioethers

are very similar to those of aliphatic thioethers.[54] The edge position of aromatic thioethers are at lower energy than the aliphatic thioethers (∼0.1 eV for (methylsulfanyl)benzene, and ∼0.5 eV for 1,1′-sulfanediyldibenzene relative to dimethyl sulfide and DL-methionine). This difference can be ascribed to the delocalization of electron density in aromatic compounds and the higher stability of excited states.

In the aromatic thioethers, the first transition has sulfur $1s \rightarrow \sigma^*(S–C)$ character, overlapped with sulfur $1s \rightarrow \pi^*(C=C)$. In (methylsulfanyl)benzene, the third transition has been replaced by pure $\sigma^*(S–C)$ excited state instead of $\pi^*(C=C)$ character in 1,1′-sulfanediyldibenzene. In 1,1′-sulfanediyldibenzene, the gas phase spectrum is the most similar to the spectrum in equilibrium geometry, and in contrast the liquid phase spectrum likely contains a mixture of different conformers, representing different interactions between the sulfur and phenyl π^* orbitals. These results show that conformation effects can be significant in analytical studies: experimental molecular models and computational studies must reflect the environment of the condensed (liquid or solid phase) to provide a correct spectroscopic interpretation.
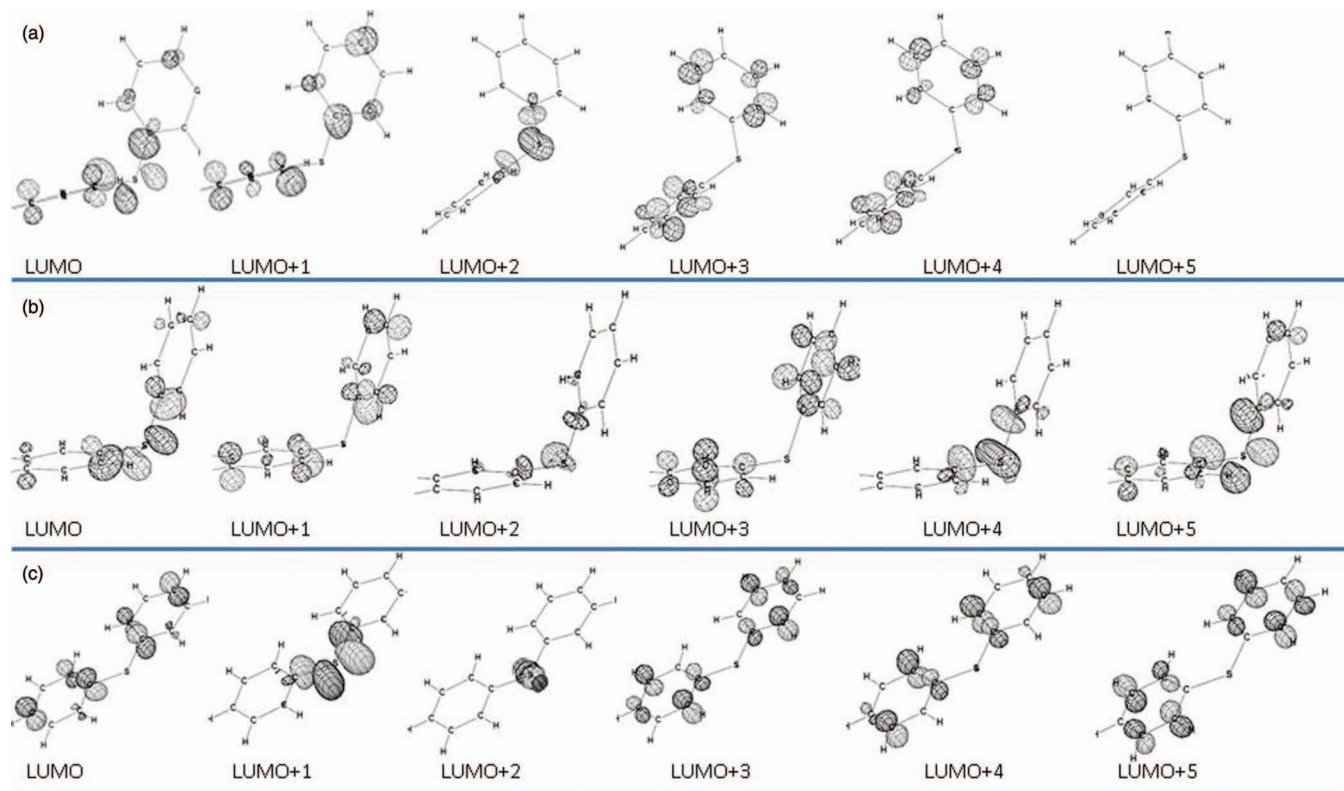
FIG. 8. Unoccupied molecular orbital diagrams for the strong features contributing to the simulated spectra obtained from Δ(SCF) calculations (a) 1,1′ sulfanediyldibenzene at equilibrium geometry; (b) 1,1′-sulfanediyldibenzene of conformer (2) from conformer 2; (c) 1,1′-sulfanediyldibenzene of conformer 3.

CONCLUSION

The NEXAFS spectra of a group of thiophenic compounds and aromatic thioethers have been obtained in gas and condensed phases and have been compared to the simulated spectra in two different levels of calculations: IVO and Δ(SCF). It was shown that Δ(SCF) calculations reproduce the experimental spectra better than IVO calculations as the spurious Rydberg-valence mixing is minimized. Calculations show that the most intense feature in the NEXAFS spectra of thiophenic compounds is from a sulfur $1s \rightarrow \sigma^*$(S–C) transition that has some π^* character from the phenyl ring. The Rydberg character decreases as the number of phenyl rings in the molecule increases. The phase of the molecules has an important role on the shape of the NEXAFS spectra. The edge position of the NEXAFS spectra moves to the higher energies in the condensed phase compared to the gas phase spectra and the white line feature becomes broader. The broadening in the condensed phase NEXAFS spectra can arise from a decrease in core excited state lifetime from quenching of the Rydberg character or increased dissociative σ^*(S–C) character.[69]

In aromatic thioethers and thiophenic compounds, the first transition is a sulfur $1s \rightarrow \sigma^*$(S–C) transition that overlaps with a sulfur $1s \rightarrow \pi^*$(C=C) character transition. In (methylsulfanyl)benzene, the last transition has been replaced by pure σ^*(S–C) excited state instead of π^*(C=C) character in 1,1′-sulfanediyldibenzene. In a previous study of aliphatic thioethers,[54] all transitions showed to have σ^*(S–C) character while in aromatic thioethers these transitions also samples the π^* density of the phenyl ring.

In summary, the modest changes in the sulfur compounds environment, including the symmetry, phase of the sample, and its functionality, can modify or shift its spectral features as it affects the mixing of atomic orbitals in the LUMOs. Conformation effects can have a significant effect in the sulfur $1s$ NEXAFS spectra of aromatic organosulfur species, providing a caution to how experimental and computational models are used to interpret analytical NEXAFS spectra.

[1]T. B. Bolin, Energy Fuels **24**, 5479 (2010).
[2]R. A. Mori, E. Paris, G. Giuli, S. G. Eeckhout, M. Kavcic, M. Zitnik, K. Bucar, L. G. M. Pettersson, and P. Glatzel, Inorg. Chem. **49**, 6468 (2010).
[3]A. Mijovilovich, L. G. M. Pettersson, S. Mangold, M. Janousch, J. Susini, M. Salome, F. M. F. de Groot, and B. M. Weckhuysen, J. Phys. Chem. A **113**, 2750 (2009).
[4]Y. Miki, M. Toba, and Y. Yoshimura, J. Jpn. Pet. Inst. **51**, 225 (2008).
[5]K. G. Kropp and P. M. Fedorak, Can. J. Microbiol. **44**, 605 (1998).

[6]N. K. Lyapina, G. N. Marchenko, M. A. Parfenova, E. G. Galkin, R. M. Nugumanov, and R. E. Grishina, Pet. Chem. **50**, 31 (2010).

[7]S. G. Mossner and S. A. Wise, Anal. Chem. **71**, 58 (1999).

[8]R. X. Hua, Y. Y. Li, W. Liu, J. C. Zheng, H. B. Wei, J. H. Wang, X. Lu, H. W. Kong, and G. W. Xu, J. Chromatogr. A **1019**, 101 (2003).

[9]A. A. H. Hegazi and J. T. Andersson, Energy Fuels **21**, 3375 (2007).

[10]F. Jalilehvand, Chem. Soc. Rev. **35**, 1256 (2006).

[11]S. Matsumoto, Y. Tanaka, H. Ishii, T. Tanabe, Y. Kitajima, and J. Kawai, Spectrochim. Acta, Part B **61**, 991 (2006).

[12]R. Wiltfong, S. Mitra-Kirtley, O. C. Mullins, B. Andrews, G. Fujisawa, and J. W. Larsen, Energy Fuels **19**, 1971 (2005).

[13]G. Sarret, J. Connan, M. Kasrai, G. M. Bancroft, A. Charrié-Duhaut, S. Lemoine, P. Adam, P. Albrecht, and L. Eybert-Bérard, Geochim. Cosmochim. Acta **63**, 3767 (1999).

[14]G. N. George, M. L. Gorbaty, S. R. Kelemen, and M. Sansone, Energy Fuels **5**, 93 (1991).

[15]G. N. George and M. L. Gorbaty, J. Am. Chem. Soc. **111**, 3182 (1989).

[16]G. Almkvist, K. Boye, and I. Persson, J. Synchrotron Radiat. **17**, 683 (2010).

[17]A. Braun, M. Janousch, J. Sfeir, J. Kiviaho, M. Noponen, F. E. Huggins, M. J. Smith, R. Steinberger-Wilckens, P. Holtappels, and T. Graule, J. Power Sources **183**, 564 (2008).

[18]P. J. Jugo, M. Wilke, and R. E. Botcharnikov, Geochim. Cosmochim. Acta **74**, 5926 (2010).

[19]Y. Fors, F. Jalilehvand, and M. Sandstrom, Anal. Sci. **27**, 785 (2011).

[20]J. Prietzel, A. Botzaki, N. Tyufekchieva, M. Brettholle, J. Thieme, and W. Klysubun, Environ. Sci. Technol. **45**, 2878 (2011).

[21]F. Allegretti, F. Bussolotti, D. P. Woodruff, V. R. Dhanak, M. Beccari, V. Di Castro, M. G. Betti, and C. Mariani, Surf. Sci. **602**, 2453 (2008).

[22]S. A. Sardar, J. A. Syed, S. Yagi, and K. Tanaka, Thin Solid Films **450**, 265 (2004).

[23]J. A. Syed, S. A. Sardar, S. Yagi, and K. Tanaka, Surf. Sci. **566**, 597 (2004).

[24]J. A. Syed, S. A. Sardar, S. Yagi, and K. Tanaka, J. Vac. Sci. Technol. A **22**, 683 (2004).

[25]J. A. Syed, S. A. Sardar, S. Yagi, and K. Tanaka, Thin Solid Films **515**, 2130 (2006).

[26]H. Modrow, G. Calderon, W. H. Daly, G. G. B. de Souza, R. C. Tittsworth, N. Moelders, and P. J. Schilling, J. Synchrotron Radiat. **6**, 588 (1999).

[27]I. Winter, J. Hormes, and M. Hiller, Nucl. Instrum. Methods Phys. Res. B **97**, 287 (1995).

[28]T. A. Smith, J. G. Dewitt, B. Hedman, and K. O. Hodgson, J. Am. Chem. Soc. **116**, 3836 (1994).

[29]A. Prange, C. Dahl, H. G. Truper, M. Behnke, J. Hahn, H. Modrow, and J. Hormes, Eur. Phys. J. D **20**, 589 (2002).

[30]I. J. Pickering, G. N. George, E. Y. Yu, D. C. Brune, C. Tuschak, J. Overmann, J. T. Beatty, and R. C. Prince, Biochemistry **40**, 8138 (2001).

[31]P. Frank, B. Hedman, and K. O. Hodgson, Inorg. Chem. **38**, 260 (1999).

[32]I. J. Pickering, R. C. Prince, T. Divers, and G. N. George, FEBS Lett. **441**, 11 (1998).

[33]A. Ito, T. Inoue, K. Takehara, N. Shimizu, Y. Kitajima, and K. Shinohara, J. X-Ray Sci. Technol. **19**, 249 (2011).

[34]A. Rompel, R. M. Cinco, M. J. Latimer, A. E. McDermott, R. D. Guiles, A. Quintanilha, R. M. Krauss, K. Sauer, V. K. Yachandra, and M. P. Klein, Proc. Natl. Acad. Sci. U.S.A. **95**, 6122 (1998).

[35]M. Howells, C. Jacobsen, T. Warwick, and A. Bos, in *Science of Microscopy*, edited by P. W. Hawkes and J. C. H. Spence (Springer, New York, 2007), pp. 835–926.

[36]G. Van der Snickt, J. Dik, M. Cotte, K. Janssens, J. Jaroszewicz, W. De Nolf, J. Groenewegen, and L. Van der Loeff, Anal. Chem. **81**, 2600 (2009).

[37]M. Cotte, E. Welcomme, V. A. Sole, M. Salome, M. Menu, P. Walter, and J. Susini, Anal. Chem. **79**, 6988 (2007).

[38]J. Prietzel, J. Thieme, U. Neuhausler, J. Susini, and I. Kogel-Knabner, Eur. J. Soil Sci. **54**, 423 (2003).

[39]K. L. I. Norlund, G. Southam, T. Tyliszczak, Y. F. Hu, C. Karunakaran, M. Obst, A. P. Hitchcock, and L. A. Warren, Environ. Sci. Technol. **43**, 8781 (2009).

[40]C. Dezarnaud, M. Tronc, and A. P. Hitchcock, Chem. Phys. **142**, 455 (1990).

[41]C. Dezarnaud, M. Tronc, and A. Modelli, Chem. Phys. **156**, 129 (1991).

[42]A. P. Hitchcock, S. Bodeur, and M. Tronc, Physica B **158**, 257 (1989).

[43]R. Chauvistre, J. Hormes, E. Hartmann, N. Etzenbach, R. Hosch, and J. Hahn, Chem. Phys. **223**, 293 (1997).

[44]A. P. Hitchcock, J. Phys. Colloques **47**, C8-575–C8-578 (1986).

[45]R. C. C. Perera and R. E. Lavilla, J. Chem. Phys. **84**, 4228 (1986).

[46]A. Mijovilovich, L. G. M. Pettersson, F. M. F. de Groot, and B. M. Weckhuysen, J. Phys. Chem. A **114**, 9523 (2010).

[47]R. Sarangi, P. Frank, K. O. Hodgson, and B. Hedman, Inorg. Chim. Acta **361**, 956 (2008).

[48]E. D. Risberg, F. Jalilehvand, B. O. Leung, L. G. M. Pettersson, and M. Sandstrom, Dalton Trans. **14**, 3542 (2009).

[49]A. P. Hitchcock, J. A. Horsley, and J. Stohr, J. Chem. Phys. **85**, 4835 (1986).

[50]H. Nakamatsu, T. Mukoyama, and H. Adachi, J. Chem. Phys. **95**, 3167 (1991).

[51]S. Bodeur, A. P. Hitchcock, and N. Kosugi, Chem. Phys. **162**, 293 (1992).

[52]E. Damian, F. Jalilehvand, A. Abbasi, L. G. M. Pettersson, and M. Sandstrom, Phys. Scr. **T115**, 1077 (2005).

[53]W. M. Kwiatek, J. Czapla, M. Podgorczyk, A. Kisiel, J. Konior, and A. Balerna, Radiat. Phys. Chem. **80**, 1104 (2011).

[54]S. Behyan, Y. F. Hu, and S. G. Urquhart, J. Chem. Phys. **134**, 244304 (2011).

[55]N. Kosugi, Theor. Chim. Acta **72**, 149 (1987).

[56]N. Kosugi and H. Kuroda, Chem. Phys. Lett. **74**, 490 (1980).

[57]R. R. Cooney and S. G. Urquhart, J. Phys. Chem. B **108**, 18185 (2004).

[58]E. Otero and S. G. Urquhart, J. Phys. Chem. A **110**, 12121 (2006).

[59]K. Ueda, M. Okunishi, H. Chiba, Y. Shimizu, K. Ohmori, Y. Sato, E. Shigemasa, and N. Kosugi, Chem. Phys. Lett. **236**, 311 (1995).

[60]S. G. Urquhart and H. Ade, J. Phys. Chem. B **106**, 8531 (2002).

[61]S. G. Urquhart, C. C. Turci, T. Tyliszczak, M. A. Brook, and A. P. Hitchcock, Organometallics **16**, 2080 (1997).

[62]S. G. Urquhart, A. P. Hitchcock, J. F. Lehmann, and M. Denk, Organometallics **17**, 2352 (1998).

[63]S. G. Urquhart, A. P. Smith, H. W. Ade, A. P. Hitchcock, E. G. Rightor, and W. Lidy, J. Phys. Chem. B **103**, 4603 (1999).

[64]E. Otero, N. Kosugi, and S. G. Urquhart, J. Chem. Phys. **131**, 114313 (2009).

[65]J. F. Lehmann, S. G. Urquhart, L. E. Ennis, A. P. Hitchcock, K. Hatano, S. Gupta, and M. K. Denk, Organometallics **18**, 1862 (1999).

[66]SPARTAN, Irvine, CA, 1994.

[67]B. Huo and A. P. Hitchcock, Simile2, Computer Program, 1996.

[68]M. O. Krause and J. H. Oliver, J. Phys. Chem. Ref. Data **8**, 329 (1979).

[69]S. G. Urquhart and R. Gillies, J. Chem. Phys. **124**, 234704 (2006).

[70]N. Kosugi, in *Chemical Applications of Synchrotron Radiation*, edited by T. K. Sham (World Scientific, 2002).

[71]A. Imanishi, T. Yokoyama, Y. Kitajima, and T. Ohta, Bull. Chem. Soc. Jpn. **71**, 831 (1998).

[72]N. Kosugi, K. Ueda, Y. Shimizu, H. Chiba, M. Okunishi, K. Ohmori, Y. Sato, and E. Shigemasa, Chem. Phys. Lett. **246**, 475 (1995).

[73]S. G. Urquhart and R. Gillies, J. Phys. Chem. A **109**, 2151 (2005).

[74]See supplementary material at http://dx.doi.org/10.1063/1.4807604 for information on Rydberg character.

[75]A. P. Hitchcock and M. Tronc, Chem. Phys. **121**, 265 (1988).

[76]M. Breinig, M. H. Chen, G. E. Ice, F. Parente, and B. Crasemann, Phys. Rev. A **22**, 520 (1980).

[77]E. D. Risberg, L. Eriksson, J. Mink, L. G. M. Pettersson, M. Y. Skripkin, and M. Sandstrom, Inorg. Chem. **46**, 8332 (2007).

[78]R. A. Mori, E. Paris, G. Giuli, S. G. Eeckhout, M. Kavcic, M. Zitnik, K. Bucar, L. G. M. Pettersson, and P. Glatzel, Anal. Chem. **81**, 6516 (2009).

[79]N. Kosugi, private communication, 2012.